Journal of Alloys and Compounds 476 (2009) 705–709

Contents lists available at ScienceDirect

Journal of Alloys and Compounds

journal homepage: www.elsevier.com/locate/jallcom

Structural transformations of $Fe_{75}Ni_2Si_8B_{13}C_2$ amorphous alloy induced by thermal treatment

D.M. Minić[a,*], A. Gavrilović[b], P. Angerer[b], D.G. Minić[c], A. Maričić[c]

[a] Faculty of Physical Chemistry, University of Belgrade, Studentski trg 12, 11001 Belgrade, Serbia
[b] ECHEM Kompetenzzentrum für angewandte Elektrochemie GmbH, A-2700 Wiener Neustadt, Austria
[c] Technical Faculty of Čačak, University in Kragujevac, Serbia

ARTICLE INFO

Article history:
Received 3 July 2008
Received in revised form 7 August 2008
Accepted 14 September 2008
Available online 1 November 2008

Keywords:
Amorphous materials
Metallic glasses
Metals and alloys
Thermal analysis
Phase transition

ABSTRACT

The structural transformations of the $Fe_{75}Ni_2Si_8B_{13}C_2$ amorphous alloy under non-isothermal as well as under isothermal conditions were studied. The amorphous alloy was stable up to a temperature of 723 K when the multi-step structural transformation began. The primary crystallization starts already at 723 K by forming Fe_xSi phase in amorphous matrix. At higher temperatures (between 780 and 800 K) beside the Fe_xSi phase, the presence of the boron–iron–silicon phase ($B_2Fe_{15}Si_3$) as well as the iron–boron (Fe_2B) phase was detected. At higher temperatures the presence of only two phases, Fe_xSi and Fe_2B, was confirmed. The Fe content in the formed Fe_xSi phase was determined as 81% (at 1273 K) and 86% (at 780 K). The kinetic parameters of crystallization processes were determined by Kissinger and Ozawa methods.

1. Introduction

The magnetic amorphous Fe–B alloys displaying excellent soft magnetic properties, such as high saturation magnetization, high permeability, low coercivity and loss, have been the subject of many scientific researches over past few decades [1]. These materials are used in diverse applications, such as power devices, information handling technology, magnetic sensors and antitheft security system [2,3].

The amorphous materials are metastable and with increase in temperature their transformation into a crystalline state occurs which can lead to change in their technologically important properties, such as the heat capacity, electrical resistivity, volume and magnetic properties [4,5].

It has been reported that either the magnetic properties may be deteriorate after crystallization or may improve if nanocrystalline phases are formed [6–9]. The commercial nanocrystalline soft magnetic materials have been successfully obtained by crystallization from amorphous precursors. These materials possess a microstructure of nanocrystals embedded in an amorphous matrix exhibiting soft magnetic properties superior to the amorphous and crystalline magnetic alloys.

In our research, we have studied the amorphous alloys based on Fe and Co, from the fundamental as well as from the practical point of view [10–13]. This paper is concerned with the thermal stability and structural transformations of $Fe_{75}Ni_2Si_8B_{13}C_2$ amorphous alloy induced by heating in the temperature range of 298–1273 K. Therefore, in order to get the optimal microstructure, a good knowledge of thermal stability and the crystallization kinetics of amorphous alloys are of significant interest for many researchers. The crystallization of these materials by heating can be performed in several ways. Usually, two basic methods can be used, isothermal and non-isothermal. The results of these measurements can then be interpreted in terms of several theoretical models [14,15].

2. Experimental procedure

The ribbon-shaped samples of $Fe_{75}Ni_2Si_8B_{13}C_2$ amorphous alloy (2 cm wide and 35 μm thick) were obtained using the standard procedure of rapid quenching of the melt on a rotating disc (melt-spinning method).

The thermal stability of the alloy as well as the structural transformations has been investigated by the differential scanning calorimetry (DSC) in a nitrogen atmosphere using a DSC-50 analyzer (Shimadzu, Japan). In this case, samples weighing several milligrams were heated in the DSC cell from room temperature to 973 K in a stream of nitrogen with a flowing rate of 20 ml min^{-1} at the different heating rates.

The amorphous structure of the as-prepared alloy sample was confirmed by X-ray diffraction (XRD) method. For the study of the transformation of structure, the samples were subsequently heated at different temperatures in the range of 623–1273 K. In order to avoid oxidation problems each sample was sealed in a

* Corresponding author. Tel.: +381 11 3336 689.
E-mail address: dminic@ffh.bg.ac.yu (D.M. Minić).

0925-8388/$ – see front matter © 2008 Elsevier B.V. All rights reserved.
doi:10.1016/j.jallcom.2008.09.072

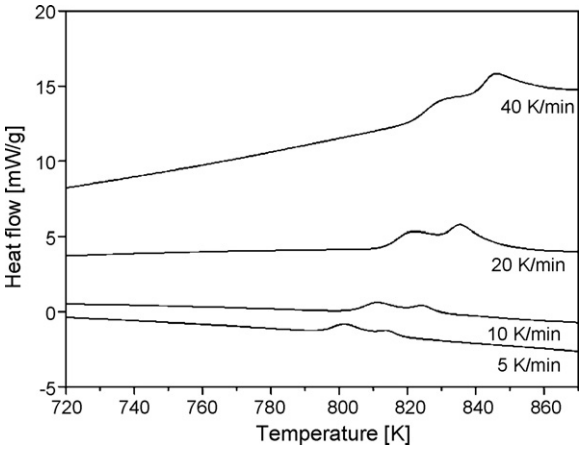

Fig. 1. Differential scanning calorimetry curves of alloy recorded at different heating rates.

quartz tube under the vacuum of 0.1 Pa and heated for 30 min at the desired temperature when it is not indicated differently. The devitrified crystalline samples were then characterized by XRD using the Cu Kα radiation at 40 kV and 30 mA in Bragg–Brentano geometry on an X-Pert powder diffractometer device (by PANalytical, Netherlands).

After the XRD measurements, the composition homogeneity of the obtained samples was inspected with a Scanning Electron Microscope (SEM) operating at 20 kV acceleration voltage. An XL 30 ESEM-FEG (environmental scanning microscope with field emission gun manufactured by FEI, Netherlands) device was used for that purpose.

3. Results and discussion

Fig. 1 shows typical DSC curves (continuous heating) for the amorphous $Fe_{75}Ni_2Si_8B_{13}C_2$ alloy taken at four different heating rates, 5, 10, 20 and 40 K min^{-1}.

All DSC curves in the temperature range of 790–860 K display the overlapping crystallization peaks, indicating the multi-stage crystallization process of the alloy. Although two peaks are detected for all the heating temperatures, their relative spacing, intensities and characteristic temperatures change with the heating rate, indicates that the heating rate has an important influence on the crystallization process. With increasing heating rate, the intensities of both peaks rise, but the intensity of the second peak increases faster. The temperature of both peaks increase with the increase of the heating rate, indicating the thermal activation of the observed steps of the crystallization process. The interval between the two peaks enlarges with the increasing heating rate as the activation energies of two crystallization processes corresponding to the exothermic peaks are different.

The overall activation energy of the crystallization reaction of an amorphous alloy, as well as the frequency factor A, under linear heating conditions can be determined by Kissinger's as well as by Ozawa's peak methods relating on the dependence of exothermic peak temperature T_p on heating rate β [16,17].

Kissinger [16] proposed that the activation energy can be determined according to the equation:

$$\ln\left(\frac{\beta}{T_p^2}\right) = \ln\left(\frac{AR}{E_a}\right) - \frac{E_a}{RT_p} \quad (1)$$

β is the heating rate, T_p is the peak temperature, A is the pre-exponential factor independent on temperature, E_a is the activation energy, and R is the gas constant.

The plot of $\ln(\beta/T_p^2)$ versus $1/T_p$ yields a straight line with a slope of $-E_a/R$ and an intercept of $\ln(AR/E_a)$.

For the determination of the activation energy in non-isothermal conditions Ozawa [17] proposed the equation:

$$\ln\ \beta = \ln\left(\frac{AE_a}{R}\right) - 1.0516\frac{E_a}{RT_p} \quad (2)$$

A plot of $\ln(\beta)$ versus $1/T_p$ yields a straight line with a slope of $-E_a/R$ and an intercept of $\ln(AE_a/R)$.

The errors of the calculated values were determined as a root-square deviation multiplied on Student's coefficient for the probability of 0.95, Table 1.

It is interesting to note the high values of the calculated activation energies of crystallization processes of the amorphous alloy, Table 1. The activation energy of solid state reactions proceeding through formation of nuclei and their growth, according to the opinion of some researchers, has no physical meaning but only empirical character and practically establishes the dependence of the rate of conversion on the temperature [11,18]. This energy can be spent not only for overcoming the activation barrier but also for co-operative displacement of atoms. Thus in these experiments, the total value of energy spent for the overcoming activation barrier as well as for co-operative displacement of atoms is determined. It should be noticed that the crystallization of amorphous alloys is a very complex process accompanied by nucleation and growth of various crystal phases under continuously varied conditions of species surroundings in a zone of conversion. Thus high values of activation energy of crystallization of amorphous alloys indicate primarily that a lot of atoms participate in an elementary process of structure reorganization, as well as the high complexity of these reactions.

The amorphous state of as-prepared alloy was confirmed by the X-ray diffraction method. The diffraction pattern of an as-prepared alloy sample, Fig. 2, shows only a spread halo in the 2θ degree range of 40–50° without appreciable diffraction peaks corresponding to crystalline phases, indicating an absence of the long-range crystalline order characteristic for an amorphous structure which remained unchanged after annealing at 623 K.

To understand the crystallization mechanism, an analysis of the X-ray diffraction patterns of the alloy heated isothermally at different temperatures, just before and above the crystallization peaks in the DSC scan (temperature range 623–1023 K) was performed. These results (cf. Fig. 2) show that the thermally induced structural changes already started at 723 K. The presence of the diffraction pattern of the Fe_xSi phase which is isotypic to gupeiite

Table 1
Kinetic parameters of both crystallization stages.

β (K min^{-1})	First stage			Second stage		
	T_p (K)	E_a (kJ mol^{-1})	ln A	T_p (K)	E_a (kJ mol^{-1})	ln A
5	801.7	380.0 ± 8 (Kissinger)	55.96 (Kissinger)	814.5	350 ± 8 (Kissinger)	51.76 (Kissinger)
10	811.4	394 ± 8 (Ozawa)	71.38 (Ozawa)	824.3	370 ± 8 (Ozawa)	51.35 (Ozawa)
20	822.0			835.6		
40	830.5			846.1		

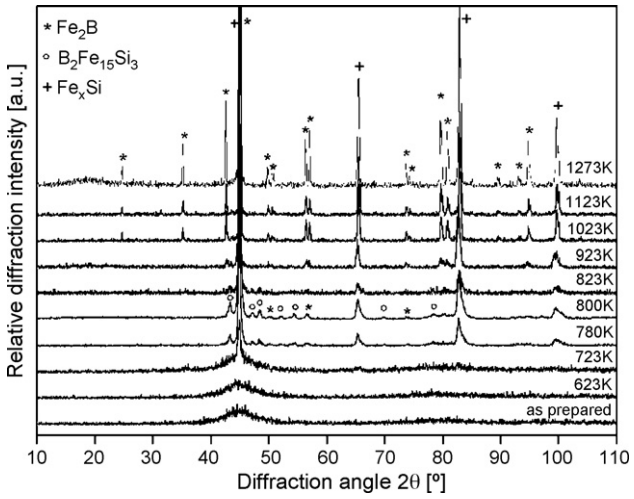

Fig. 2. X-ray diffraction patterns the as-prepared alloy and after thermal treatment at given temperatures.

(JCPDS-PDF 03-065-0146) together with the halo from a residual amorphous phase in the diffraction angle range of 40–50° indicates that isothermal heating at 723 K during 30 min caused the partial crystallization of the Fe_xSi phase in an amorphous matrix. At higher temperatures (780 K) beside the intense diffraction pattern of the Fe_xSi phase, weak peaks of the boron–iron–silicon phase ($B_2Fe_{15}Si_3$), corresponding to JCPDS-PDF 00-047-1629 and of the iron boron (Fe_2B) phase according to [JCPDS-PDF 03-065-2693] became visible. At 923 K the intensity of the iron–boron peaks increased, while the peaks of the boron–iron–silicon phase completely disappeared.

Furthermore, increase of the heating temperature, as well as the extension of heating time, leads to the increase of intensities all present peaks pointing to the better crystallization of all present phases, Fig. 3 and Table 2. It is clear that after the final crystallization stage at 1123 K (cf. Figs. 2 and 3), only two phases are present: iron–boron (Fe_2B) and iron–silicon (Fe_xSi).

The diffraction angles of the characteristic peaks for the Fe_xSi phase display a slight shifting due to the variation of the lattice parameter *a*. In Fig. 4 the relation between the Fe content (or Fe/Si ratio) and the lattice constant *a* is plotted (data given according to JCPDS 35-519, 1071-4480,1071-6175, 3065-3192, 3065-6323, 3065-9130). The line corresponds to a parabolic regression curve which was used for the calculation of the Fe content. The shaded bar in the diagram in Fig. 4 corresponds to the observed range of composition. From this relation the Fe content between 81% (observed at 1273 K) and 86% (at 780 K) of the Fe_xSi phase could be deduced. However, no clear relation between the Fe content and the corresponding annealing temperature of the sample could be deduced. It should also be noted that a possible variation of the Fe/Si ratio in the sample can influence the width of the diffraction maxima which consequently can inhibit the precise determination of the crystallite size of this phase.

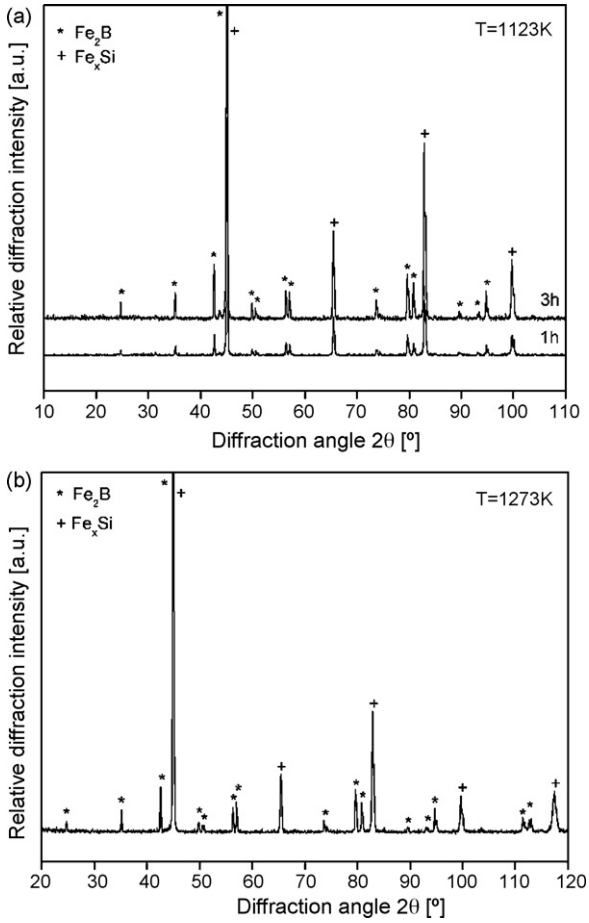

Fig. 3. X-ray diffraction patterns of $Fe_{75}Ni_2Si_8B_{13}C_2$ alloy samples heated: (a) during 1 h and 3 h at 1123 K, and (b) during 3 h at 1273 K.

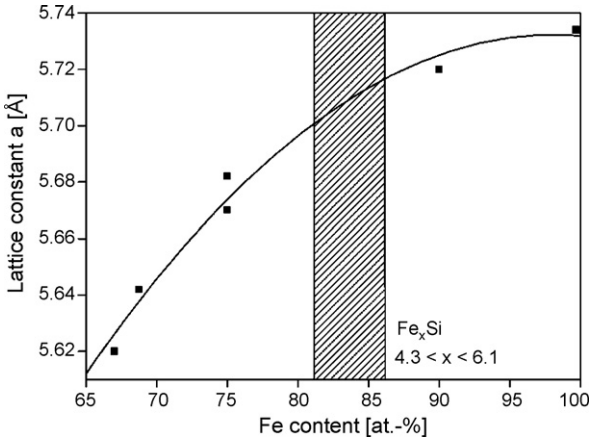

Fig. 4. Lattice constant for various Fe_xSi compounds as given in JCPDS database plotted as a function of the stoichiometric Fe content.

Table 2
Phase composition of alloy $Fe_{75}Ni_2Si_8B_{13}C_2$ as found by XRD analysis. Data for lattice parameters corresponding to the JCPDS-PDF data.

Phase	Formula	Space group	Crystal system	Lattice parameters (Å)	
				a	*c*
Iron–boron	Fe_2B	I-42m	Tetragonal	5.099	4.240
Iron–silicon	Fe_3Si	Fm-3m	Cubic	5.670	–
Boron–iron–silicon	$B_2Fe_{15}Si_3$	I-4	Tetragonal	8.677	4.307

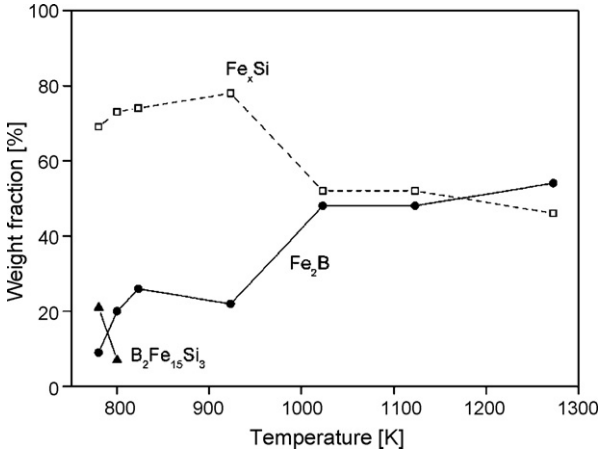

Fig. 5. Weight fraction as determined by Rietveld's refinement method.

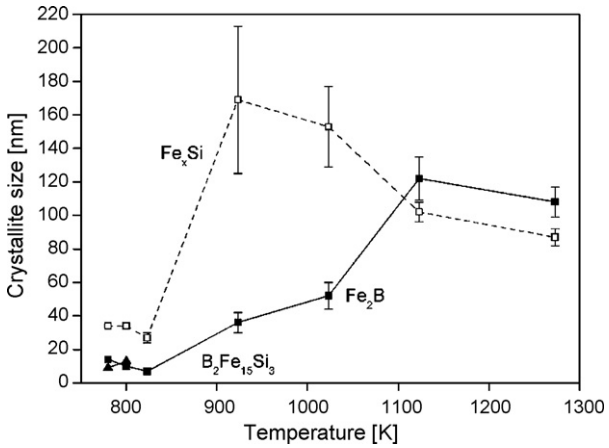

Fig. 6. Change of the crystallite size of phases formed during the isothermal heating of $Fe_{75}Ni_2Si_8B_{13}C_2$ amorphous alloy.

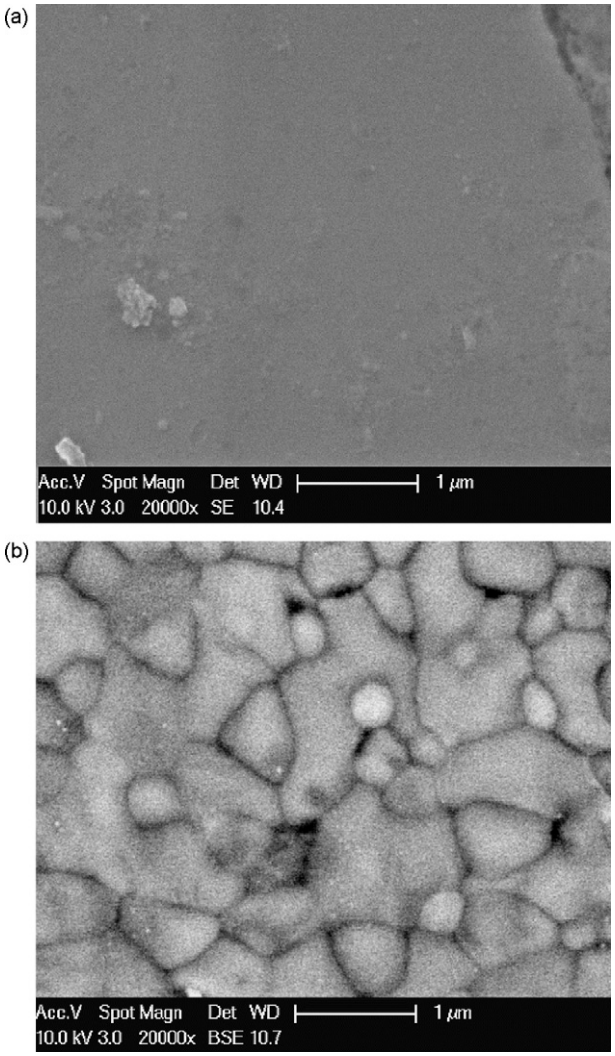

Fig. 7. Scanning electron micrograph images of the sample surface: (a) before heating and (b) after heat treatment at 1273 K during 1 h.

For the qualitative determination of the phase composition of the crystallized alloy samples the JCPDS-PDF database has been used. Besides the phase composition the quantitive calculation of the contents of each individual phase is essential. Rietveld's refinement procedure is able to simulate the XRD pattern from given starting parameters. The purpose of this simulation is therefore to refine individual parameters, e.g. phase content, crystallite size, and crystal lattice parameters, to obtain a good fit. For this purpose Rietveld's refinement program TOPAS V3.0 (Bruker AXS GmbH, Germany) was used [19]. This software enables the full handling of the instrument geometry and the instrument profile parameters. The quality of the refinement progress was controlled by monitoring the fit parameter R_{wp}, the goodness of fit (GOF), and the Durbin–Watson factor. Besides, the values for the weight fraction for each phase in the penetrated sample volume (cf. Fig. 5), the values for the crystallite size and the microstrain, were determined by Rietveld's method as well (see Table 3). The contents of iron–boron, iron–silicon and boron–iron–silicon phase are displayed as a function of the annealing temperature during the heating experiment. However it should be remarked that the first appearance of the Fe_xSi phase at 723 K is not covered in the diagram in Fig. 5 because the amorphous phase coexisting at this temperature inhibits the correct phase content determinated by Rietveld's method.

The change of the crystallite dimensions, D_{hkl}, the dislocation density, ρ_{hkl}, and microstrains, ε_{hkl}, of formed phases with increas-

Table 3
Crystallite size, dislocation density and microstrain of alloys heated at different temperatures.

Temperature (K)	Boron–iron		Boron–iron–silicon		Iron–silicon		ε_{hkl} (%)
	D_{hkl} (nm)	ρ_{hkl} (m^{-2})	D_{hkl} (nm)	ρ_{hkl} (m^{-2})	D_{hkl} (nm)	ρ_{hkl} (m^{-2})	
780	14	1.53×10^{16}	9	3.70×10^{16}	34	2.60×10^{15}	9.72
800	10	3.00×10^{16}	13	1.78×10^{16}	34	2.60×10^{15}	7.88
823	7	6.12×10^{16}	–	–	27	4.12×10^{15}	7.35
923	36	2.32×10^{15}	–	–	169	1.05×10^{14}	2.74
1023	52	1.11×10^{15}	–	–	153	1.28×10^{14}	1.15
1123	122	2.02×10^{14}	–	–	102	2.88×10^{14}	0.46
1273	108	2.57×10^{14}	–	–	87	3.96×10^{14}	1.32

ing temperature of heating are shown in Table 3. It shows that the crystallization process starts with nanosized crystallites, and their growth is further temperature dependent, Fig. 6.

The samples were inspected before and after heat treatment by scanning electron microscopy (SEM) using 20 kV acceleration voltage. All SEM micrographs are displayed at the same magnification. Fig. 7a shows the amorphous sample before heat treatment. It is clear that the as-prepared sample surface is homogeneous, without any trace of prior nucleation. A SEM micrograph in Fig. 7b displays different grain sizes in the range from about 0.3 to 2 μm. These dimensions are significantly bigger than the dimensions we obtain from X-ray diffraction pattern in Table 3. The SEM micrograph represents particles consisting from several crystallites (mosaic structure) non-accessible to the X-ray diffraction which is strictly related to the smaller coherent diffracting length. However, the scanning electron microscopic examination of the sample heated at the highest temperature revealed the presence of three different particle sizes. The smallest, almost spherical particles with a grain size in a range of 0.3–0.5 μm, correspond to the iron silicon phase; the largest particles (with a grain diameter between 1 and 2 μm) are related to the Fe_2B phase. Well-defined particles with a medium size (0.5–0.7 μm) probably correspond to the iron–silicon phase as well.

4. Conclusions

By annealing in the temperature range 298–1273 K, the amorphous $Fe_{75}Ni_2Si_8B_{13}C_2$ alloy undergoes multi-step structural transformations, forming iron–silicon (Fe_xSi), iron–silicon–boron ($B_2Fe_{15}Si_3$) and iron–boron (Fe_2B) phases. The primary crystallization starts at 723 K by forming Fe_xSi phase in an amorphous matrix. At higher temperatures (780 and 800 K) beside the Fe_xSi phase, weak peaks of the boron–iron–silicon phase ($B_2Fe_{15}Si_3$) and of the iron–boron (Fe_2B) phase became visible. At 923 K the intensity of the iron–boron peaks increased, while the peaks of the boron–iron silicon phase completely disappeared. From the relation between the Fe content and the lattice constant *a*, the Fe content in the Fe_xSi phase was determined as 81% (observed at 1273 K) and 86% (at 780 K). The crystallization process starts with nanosized crystallites, and their growth is further temperature dependent.

Acknowledgements

The investigation was partially supported by the Ministry of Science and Environmental Protection of Serbia, under the following Project and 142025. The work at ECHEM was supported within the K plus programme by the Austrian Research Promotion Agency (Österreichische Forschungförderungsgesellschaft, FFG) and the government of Lower Austria.

References

[1] K. Biswas, S. Ram, L. Schultz, J. Eckert, J. Alloy Compd. 397 (2005) 104.
[2] I.C. Ho, C.S. Yoon, C.K. Kim, T.Y. Byun, K.S. Hong, Mater. Sci. Eng. B 96 (2002) 48.
[3] T. Gloriant, S. Surinah, M.D. Baro, J. Non-Cryst. Solids 333 (2004) 320.
[4] A.A. Soliman, S. Al-Heniti, A. Al-Hajry, M. Al-Assiri, G. Al-Barakati, Thermochim. Acta 413 (2004) 57.
[5] H.F. Li, R.V. Ramanujan, Thin Solid Films 514 (2006) 316.
[6] D.M. Minić, A.M. Maričić, R.Z. Dimitrijević, M.M. Ristić, J. Alloy Compd. 430 (2007) 241.
[7] H.F. Li, R.V. Ramanjujan, Mater. Sci. Eng. A 375 (377) (2004) 1087–1091.
[8] J. Bednarick, R. Nicula, M. Stir, E. Bukel, J. Magn. Magn. Mater. 316 (2007) e823.
[9] M.E. Mchenry, M.A. Willard, D.E. Laughlin, Prog. Mater. Sci. 44 (1999) 291.
[10] T. Žak, O. Schneeweiss, D. Minić, J. Magn. Magn. Mater. 272–276 (2004) e1119.
[11] D.M. Minić, A. Maričić, R.Z. Dimitrijević, M.M. Ristić, J. Alloy Compd. 430 (2007) 242.
[12] D.M. Minić, A. Maričić, B. Adnadjević, J. Alloy Compd. (2008), doi:10.1016/j.jalcom.2008.05.087.
[13] D.M. Minić, B. Adnadjević, Thermochim. Acta 424 (2008) 41.
[14] D.W. Handerson, J. Non-Crystal. Solids 30 (1970) 301.
[15] K. Matusita, S. Sakka, J. Non-Crystal. Solids 38 (39) (1980) 741.
[16] H.E. Kissinger, Anal. Chem. 29 (1957) 1702.
[17] T. Ozawa, J. Ther. Anal. 29 (1970) 301.
[18] S.D. Kaloshkin, I.A. Tomilin, Thermochim. Acta 280–281 (1996) 303.
[19] Bruker AXS, TOPAS V3: General profile and structure analysis software for powder diffraction data, Karlsruhe, 2005.